Railway Wheelset Active Control and Stability via Higher Order Neural Units

Peter Mark Benes and Ivo Bukovsky ⓘ, *Senior Member, IEEE*

Abstract—This article investigates an unconventional approach to solving the control of lateral displacement for railway bogie wheelsets using recurrent higher order neural units (HONUs). Although studies addressing control of independently rotating wheelsets have shown promising results, they are rarely applied by railway manufacturers. Research and developments in modern bogie design are trending toward active yaw control design as an extension to conventional wheelsets mechanics, particularly for higher speeds. We investigate a model-reference architecture for active control via setpoint tracking of lateral displacement. Then, a new HONU sliding mode architecture is derived to solve convergence for zero lateral displacements in higher running speeds which is a more profoundly complex issue in maintaining minimal hunting motion. Starting from the property of nonlinear polynomial architecture of HONUs with in-parameter linearity, we derive a time-variant state-space representation via nonlinear identical decomposition. Then, an input-to-state stability (ISS) approach is applied to prove the local asymptotic convergence of the applied algorithm in each state point and the bounded-input-bounded-state stability of the entire nonlinear adaptive control loop. Using ISS theory, we also prove the global asymptotic stability of the HONU sliding mode controller for the actively controlled wheelset system. The techniques are validated by simulations and a real roller rig system.

Index Terms—Bounded-input-bounded-state, conventional (rigid) wheelset, discrete-time polynomial systems, higher order-neural-units, independently rotating wheels (IRW), input-to-state stability (ISS), sliding mode control.

Peter Mark Benes is with the Rail Automation Division R&D, Siemens Mobility s.r.o., 155 00 Prague, Czech Republic (e-mail: peter.benes@siemens.com).

Ivo Bukovsky is with the Department of Computer Science, Faculty of Science, University of South Bohemia in České Budějovice, 370 05 České Budějovice, Czech Republic, and also with the Department of Mechanics, Biomechanics, and Mechatronics, Faculty of Mechanical Engineering, Czech Technical University in Prague, 370 05 Prague, Czech Republic (e-mail: ibukovsky@ieee.org).

I. INTRODUCTION

ACTIVELY guided wheelsets for railway vehicle bogie systems are considered one of the most advanced concepts for future rail transportation because they ultimately minimize the lateral forces and damage to wheel flanges and rail heads [1]. Compared to conventional passive bogie frames and wheelset designs, better performance can be achieved in terms of stability, curving behavior, and passenger comfort [2]. Several works in active wheelset control for a conventional wheelset configuration have shown promising results [3], [4], [5]. However, it is an ongoing challenge to reduce hunting motion, especially with increased running speeds. More demandingly is the further control challenge of robust performance with independently rotating wheels (IRWs). However, the application of IRW configurations is still quite rare in modern rail bogie manufacturing, so the focus is more pragmatically toward active control mechanisms as an extension to existing conventional wheelset design [6]. Apart from conventional control results utilizing state-feedback design [7], [8] and further methods for yaw torque control [9], this article investigates a computational intelligence approach with higher order neural units, which is quite novel considering main recent works till now rather focused towards measurement problems [10], or focused to other applications like automotive wheelset control [11]. The advantage of computational intelligence approaches is the adaptability to both real-time linear and nonlinear dynamical changes, such as mechanical wear and track irregularities or curvatures. Further that being a data driven method, system dynamics can be identified even with limited measurement of all dynamical states or precise mathematical descriptions.

Recent works, e.g., [12], [13], [14], demonstrate the usefulness and efficiency of computational intelligence tools applied to model reference adaptive control (MRAC). MRAC is one of the fundamental modern control schemes using neural networks (among the others such as model predictive control or reinforcement learning, i.e., adaptive dynamic programming). The drawback of multi-layered neural networks is that they require rather complex training algorithms or longer training to achieve reasonable convergence to a minimum squared error for solving local minimum problems [15]. Other, more conventional neural network architectures, such as radial basis function networks, have also been shown to be successful in reinforcement learning control schemes [16], [17]. The approximation strength of such conventional neural networks is enforced by adding more neurons or even additional layers. Nowadays, this appears useful

with very complex and large (deep) networks, where the desired network behavior emerges among the vast number of neurons and high training effort.

However, we often lack high-quality training and validation data in real dynamic systems and technological processes. Therefore, smaller and easier-to-analyze neural models and controllers are often desirable, especially for real-time applications. Therefore, we propose the use of HONUs with efficient real-time learning algorithms, such as the gradient descent algorithm [18], recursive least squares algorithm (RLS), and Levenberg–Marquardt (L-M) batch algorithm [19] as such comprehensible and efficient learning algorithms for application to active control. As an extension of our original work on the problem [20], [21] with model-reference based architecture (HONU-MRAC), a newly proposed sliding mode approach is also derived using notions from [17] and [22] and earlier concepts in [23] and [24] to solve zero convergence of lateral displacement particularly at higher speeds, different to the control objective of setpoint tracking which is typical for model reference-based approaches and can be computationally more efficient with the reduction to a single neural unit (single HONU) for dynamic identification.

Another challenge in developing any control architecture is proving or monitoring the stability of the control loop both as an online adaptive solution and offline tuned solution using newly identified dynamic data. A traditional approach is to construct the adaptive control law via a suitable Lyapunov function candidate to ensure a global rule to constrain the process inputs. In cases where the law is used as an optimizer for an existing control loop, bounded-input bounded-state (BIBS) stability [25] can be used with a more universal definition of input-to-state stability (ISS) [26] to prove stability of the entire loop. ISS and BIBS-based stability analyses are a practical means of ensuring stability and online monitoring for online tuned and offline applied architectures. Therefore, this is a suitable justification for our proposed control scheme with HONUs.

The article is organized as follows. Section II introduces the investigated bogie wheelset system. Section III investigates the use of the HONU-MRAC based control architecture for setpoint tracking of the lateral displacement of the wheelset. Based on the fundamental nonlinear polynomial architecture of HONUs and theories of ISS stability, a HONU sliding mode architecture is then derived for solving zero lateral displacement convergence with minimized hunting motion, which remains particularly complex at increased speeds. After proof of stability for the proposed control architectures in Section IV, experimental results are shown on a real scaled experimental wheelset and bogie frame system (roller rig) in Section V to prove the applicability of the proposed methods for various conditions in real rail applications. In math notations, vectors and matrices are bold, plain y represent real values, and tilde $\tilde{y}$ denotes neural output.

II. INVESTIGATED WHEELSET AND BOGIE SYSTEM

The investigated wheelset and bogie frame (see Fig. 1) on roller system can be defined via the following equations of motion, as a modification from [27] and [28] for two solid axle
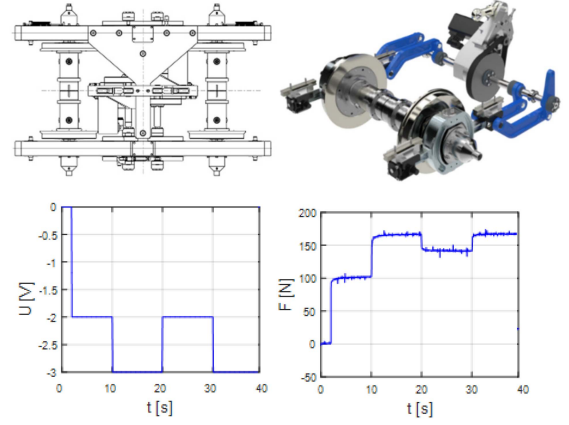

Fig. 1. (Top): actuated wheelset plan view and assembly of roller rig system. (Bottom): measured actuator force with lateral counter force in relation to applied driving voltage (control input).

wheelsets and steering of leading wheelset as follows:

$$m \cdot \ddot{y}_{w1} = \left[\frac{-2f_{22}}{V} - C_w\right]\dot{y}_{w1} - K_w \cdot y_{w1}$$
$$+ 2f_{22} \cdot \Psi_{w1} + C_w \cdot \dot{y}_{b1}$$
$$+ K_w \cdot y_{b1} + C_w \cdot l_b \cdot \dot{\Psi}_{b1} + K_w \cdot l_b \cdot \Psi_{b1}$$
$$+ F_{y1} + \frac{mV^2}{R_0} + mg\vartheta - F_{c1} \;, \tag{1}$$

$$I_w\ddot{\Psi}_{w1} = \frac{-2f_{11} \cdot l \cdot \lambda}{r}y_{w1} - \frac{2f_{11} \cdot l^2}{V}\dot{\Psi}_{w1} + T_{\Psi 1} \tag{2}$$

and with the trailing wheelset given as follows:

$$m \cdot \ddot{y}_{w2} = \left[\frac{-2f_{22}}{V} - C_w\right]\dot{y}_{w2} - K_w \cdot y_{w2}$$
$$+ 2f_{22} \cdot \Psi_{w2+} + C_w \cdot \dot{y}_{b1}$$
$$+ K_w \cdot y_{b1} - C_w \cdot l_b \cdot \dot{\Psi}_{b1} - K_w \cdot l_b \cdot \Psi_{b1} + F_{y2}$$
$$+ \frac{mV^2}{R_0} + mg\vartheta - F_{c2}, \tag{3}$$

$$I_w\ddot{\Psi}_{w2} = \frac{-2f_{11}l\lambda}{r}y_{w2} - \frac{2f_{11}l^2}{V}\dot{\Psi}_{w2} + T_{\Psi 2} \tag{4}$$

where assuming the steering mechanism frame in Fig. 1 is fixed to the reference frame for independent translation of the actuator torques. Furthermore, simplification of the sinus relation of track cant at smaller angles. Then, the relations for the surrounding bogie frame can be defined as follows:

$$m_b \cdot \ddot{y}_{b1} = C_w \cdot \dot{y}_{w1} + K_w \cdot y_{w1} + C_w \cdot \dot{y}_{w2} + K_w \cdot y_{w2}$$
$$- 2C_w \cdot \dot{y}_{b1} - 2K_w \cdot y_{b1} - \frac{2mV^2}{R_0} - 2mg\vartheta \;, \tag{5}$$

$$I_b \cdot \ddot{\Psi}_{b1} = C_w \cdot l_b \cdot \dot{y}_{w1} + K_w \cdot l_b \cdot y_{w1}$$
$$- C_w \cdot l_b \cdot \dot{y}_{w2} - K_w \cdot l_b \cdot y_{w2}$$
$$- 2C_w \cdot l_b^2 \cdot \dot{\Psi}_{b1} - 2K_w \cdot l_b^2 \cdot \Psi_{b1} + (F_{c1} - F_{c2}) \cdot l_b. \tag{6}$$
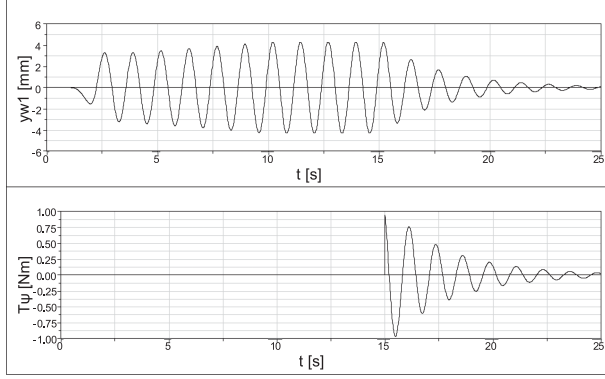
Fig. 2.   (Top): conventional wheelset response under applied input yaw torque (Bottom) $T_{\Psi}\ [Nm]$ (control input) followed by state feedback control at $t = 15$ s on simulation of roller rig system from [8].

The parameters are set as follows: wheelset mass m, bogie frame mass m_b, longitudinal creep coefficient f_{11}, lateral creep coefficient f_{22}, wheelset yaw inertia I_w, bogie yaw inertia I_b, half distance of the rolling circle l, half wheelbase l_b, wheel conicity λ, wheelset radius r, curve radius R_0, track cant ϑ, and rotational speed V. On setting the value f_{11} to be negligibly small (almost zero), these relations may also be used to describe a simplified IRW configuration. Then, although numerous advanced works on nonlinear lateral forces due to wheel flange and rail contact exist, e.g., [29]. For scope of our simulations a simplified model, where the wheel flanges are limited at $\pm\,6$ mm of lateral displacement can be drawn from the empirical norm relation [30], [31] as follows:

$$F_{c1,2} =$$
$$\begin{cases} p \cdot c_{f1} \left(1 - e^{-0.25 \cdot \Psi_{w1,2}}\right) \cdot \sum_{i=0}^{n=2} F_{wi}, & if -6 > y_{w1,2} > 6 \\ 0, & if -6 \leq y_{w1,2} \leq 6 \end{cases},$$
$$(7)$$

where c_{f1} is the frictional coefficient factor of the wheel flanges and the yaw displacement is expressed in mm/m. F_{wi} then depicts the sum of static wheel loads on each wheel and p is the position force factor expressed as a ratio of bogie span to wheelbase. Then, knowing the lateral span of the wheelset steering linkages w the conversion of driving voltage into control input (yaw torque) maybe measured via Fig. 1 as $T_{\Psi 1} = F_{\Psi 1}/2w$, incorporating any lateral counter force from rail contact. Another nonlinear saturation is considered to keep the driving voltage between $\pm\,6$ V; the controlled output is the leading wheelset lateral displacement $y_{w1} = y$ with respect to the absolute reference frame (i.e., track).

Fig. 2 illustrates the dynamics of the railway bogie for conventional wheelset configurations with state feedback active control switched ON during motion, as a benchmark for comparison. Significant hunting motion is already visible in the conventional wheelset configuration due to conicity of the wheel profiles, where under active control the effects are minimized to almost 0 mm in 10 s.

III. PROPOSED HONU FRAMEWORK FOR ACTIVE CONTROL

A. HONU-MRAC Control Architecture

As it may be recalled from [24] and [32], the classical notation of HONUs has been $\Sigma\Pi$ form, where the example of second-order HONU, i.e., QNU, is as follows:

$$\tilde{y} = \sum_{i=0}^{n} \sum_{j=i}^{n} w_{i,j} \cdot x_i \cdot x_j \qquad (8)$$

where $\tilde{y}$ is neural output and the augmented input vector is as follows:

$$\mathbf{x}(k) = \begin{bmatrix} x_0 & x_1 & \dots & x_i & x_{i+1} & \dots & x_n \end{bmatrix}^T \qquad (9)$$

where $x_0 = 1$ is the augmenting unit for neural bias, and that also allows HONUs for lower order polynomial terms, $w_{i,j}$ are neural weights of QNU, and $^{\mathrm{T}}$ denotes vector transposition.

Since recently in [32], long vector form of HONUs was proposed via operators $\mathrm{col}^r(\mathbf{x})$ and $\mathrm{row}^r(\mathbf{x})$, e.g., it is for QNU as follows:

$$\tilde{y} = \mathbf{w} \cdot \mathrm{col}^{r=2}(\mathbf{x}) = \mathrm{row}^{r=2}(\mathbf{x}) \cdot \mathbf{w}^T \qquad (10)$$

or for CNU as follows:

$$\tilde{y} = \mathbf{w} \cdot \mathrm{col}^{r=3}(\mathbf{x}) = \mathrm{row}^{r=3}(\mathbf{x}) \cdot \mathbf{w}^T \qquad (11)$$

where the operators $\mathrm{col}^r(\mathbf{x})$ and $\mathrm{row}^r(\mathbf{x})$ transform input vector $\mathbf{x}$ into a long vector of polynomial terms, i.e., into a long-column vector for QNU as follows:

$$\mathrm{col}^{r=2}(\mathbf{x}) = \{ \ x_i \cdot x_j \ ; \quad i = 0 \dots n, \ j = i \dots n\} \qquad (12)$$

or into a long-row vector for CNU as follows:

$$\mathrm{row}^{r=3}(\mathbf{x}) = \{ \ x_i \cdot x_j \cdot x_\kappa \ ; \quad i = 0 \dots n \ , \ j$$
$$= i \dots n \ , \quad \kappa = j \dots n\}. \qquad (13)$$

Further in (10) and later on, w is the long-vector of all neural weights (i.e., r-dimensional $\mathbf{W}$ also flattens into one-dimensional vector w) and for the example of QNU it is as follows:

$$\mathbf{w} = \begin{bmatrix} w_{0,0} & w_{0,1} & \dots & w_{i,j} & \dots & w_{n,n} \end{bmatrix}$$
$$= \begin{bmatrix} \{w_{i,j}\} & \begin{matrix} i = 0 \dots n \\ j = i \dots n \end{matrix} \end{bmatrix} \qquad (14)$$

and similarly flattened long vectors of neural weights are used for higher polynomial orders. The weight-update is then generally given as follows:

$$\mathbf{w}(k) = \mathbf{w}(k - 1) + \Delta\mathbf{w} \qquad (15)$$

where k denotes sample index or can be replaced with epoch index for batch learning. Then, the augmented input vector of the recurrent HONU in the forward branch is as follows:

$$\mathbf{x}(k) = [1 \ \tilde{y}(k - n_y + 1) \ \dots \ \tilde{y}(k) \ u(k - n_u + 1) \ \dots \ u(k)]^T \qquad (16)$$

where $\tilde{y}$ is the forward-branch HONU output and u is the control input.
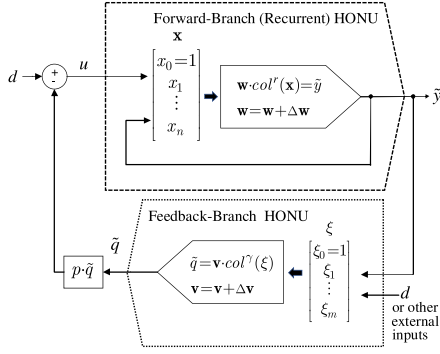
Fig. 3. HONU-MRAC control loop (where one HONU is as a plant model and the second as a feedback controller).

The feedback control law may then be defined in Fig. 3 as follows:

$$u(k) = d(k) - p(k) \cdot \tilde{q}(k) \tag{17}$$

where $\tilde{q}(k)$ is an output of the feedback-branch HONU defined in (18), $d(k)$ can be desired value, and $p(k)$ is an adaptable proportional gain. The feedback-branch HONU output $\tilde{q}$ is defined as follows:

$$\tilde{q}(k) = \mathbf{v}(k) \cdot \mathrm{col}^\gamma(x(k)) \tag{18}$$

where $\mathbf{v}$ is the long vector of weights, ξ is a customizable input vector involving step delays of $\tilde{y}$ and u with the augmenting unit $\xi_0 = 1$, and γ is the customizable nonlinear polynomial order of the feedback-branch HONU.

In following sections, we justify stability of the approach for both standalone recurrent HONUs and for the HONU-MRAC configuration shown in Fig. 3 as offline tuned and online adaptive form.

Recurrent HONUs and their dynamical structures can be decomposed into a nonlinear state-space representation that conforms with the ISS stability definition (50), or, e.g., [26], so the stronger BIBS stability can be defined for HONUs later in Section IV, via the so-called discrete-time dynamic HONU stability (DDHS) method. Let us consider a recurrent discrete time HONU of an arbitrary order r as follows:

$$\tilde{y}(k) = \mathbf{w}(k) \cdot \mathrm{col}^r(\mathbf{x}(k-1)); \mathbf{x}(k-1) = \begin{bmatrix} 1 \\ \hat{\mathbf{x}}(k-1) \\ \hat{\mathbf{u}}(k-1) \end{bmatrix} \tag{19}$$

where the elements of vector $\mathbf{x}$ are defined as follows:

$$\hat{\mathbf{x}}(k-1) = \begin{bmatrix} \tilde{y}(k-n_y) & \tilde{y}(k-n_y+1) & .. & \tilde{y}(k-1) \end{bmatrix}^T, \tag{20}$$

$$\hat{\mathbf{u}}(k-1) = \begin{bmatrix} u(k-n_u) & u(k-n_u+1) & \ldots & u(k-1) \end{bmatrix}^T. \tag{21}$$

The summation form of QNU (and similarly for higher polynomial orders), can be restated in subpolynomial form as follows:

$$\tilde{y}(k) = \sum_{i=0}^{n} \sum_{j=i}^{n} w_{i,j} \cdot x_i \cdot x_j = w_{0,0}$$

$$+ \sum_{i=1}^{n_y} x_i \cdot \left(w_{0,i} + \sum_{j=i}^{n} w_{i,j} \cdot x_j \right)$$

$$+ \sum_{i=n_y+1}^{n} x_i \cdot \left(w_{0,i} + \sum_{j=i}^{n} w_{i,j} \cdot x_j \right) \tag{22}$$

where $n = n_y + n_u$ when considering (19)–(21) and thus the QNU, for example, yields

$$\hat{x}_{n_y}(k) = w_{0,0} + \sum_{i=1}^{n_y} \hat{x}_i(k-1) \cdot \hat{a}_i + \sum_{i=1}^{n_u} \hat{u}_i(k-1) \cdot \hat{b}_i \tag{23}$$

where $\hat{a}_i$ are decomposition coefficients as follows:

$$\hat{a}_i = \hat{a}_i(\hat{\mathbf{x}}(k-1), \hat{\mathbf{u}}(k-1), \mathbf{w}) = w_{0,i} + \sum_{j=i}^{n} w_{i,j} \cdot x_j(k-1) \tag{24}$$

where $x_j \in \mathbf{x}$ was defined in (19), and similarly, the decomposition coefficients with only input terms are as follows:

$$\hat{b}_i = \hat{b}_i(\hat{\mathbf{u}}(k-1), \mathbf{w}) = w_{0,i} + \sum_{j=i \; ; \; i>n_y}^{n} w_{i,j} \cdot x_j(k-1). \tag{25}$$

With the decomposition coefficients (24) and (25) and given the definition of state vector (20) and input vector (21), we may express recurrent HONUs in a canonical state-space form as follows:

$$\hat{\mathbf{x}}(k) = \hat{\mathbf{A}}(k-1) \cdot \hat{\mathbf{x}}(k-1) + \hat{\mathbf{B}}_\mathbf{a} \cdot \hat{\mathbf{u}}_\mathbf{a}(k-1);$$
$$\tilde{y}(k) = \hat{\mathbf{C}} \cdot \hat{\mathbf{x}}(k) \tag{26}$$

where

$$\hat{\mathbf{A}}(k) = \hat{\mathbf{A}}(\hat{\mathbf{x}}, \hat{\mathbf{u}}, \mathbf{w}, k) = \begin{bmatrix} 0 & 1 & 0 & \cdots & 0 \\ 0 & 0 & 1 & \cdots & \vdots \\ 0 & 0 & \ddots & \ddots & 0 \\ 0 & 0 & \ddots & 0 & 1 \\ \hat{a}_{n_y} & \hat{a}_{n_y-1} & \cdots & \hat{a}_2 & \hat{a}_1 \end{bmatrix}. \tag{27}$$

$\hat{\mathbf{A}}$ is the time-variant local matrix of dynamics (LMD) and $\hat{\mathbf{B}}_\mathbf{a} = \hat{\mathbf{B}}_\mathbf{a}(\hat{\mathbf{u}}, \mathbf{w}, k)$ is (also time-variant) augmented local input matrix, and the neural bias weight $w_{0,0} = w_{0,0}(k)$ is treated as another input, so the augmentation is

$$\hat{\mathbf{B}}_\mathbf{a}(k) = \hat{\mathbf{B}}_\mathbf{a}(\hat{\mathbf{u}}, \mathbf{w}, k) = \begin{bmatrix} & & 0 \\ \hat{\mathbf{B}} & & \vdots \\ & & 0 \\ & & 1 \end{bmatrix},$$

$$\hat{\mathbf{u}}_\mathbf{a}(k-1) = \begin{bmatrix} \hat{\mathbf{u}}(k-1) & w_{0,0}(k-1) \end{bmatrix}^T \tag{28}$$

where $\hat{\mathbf{u}}$ was defined in (21) and further

$$\hat{\mathbf{B}} = \begin{bmatrix} 0 & 0 & \cdots & 0 \\ \vdots & \vdots & \ddots & \vdots \\ 0 & 0 & \cdots & 0 \\ \hat{b}_{n_u} & \hat{b}_{n_u-1} & \cdots & \hat{b}_1 \end{bmatrix}, \hat{\mathbf{C}} = \begin{bmatrix} 0 & \cdots & 0 & 1 \end{bmatrix}^T.$$

(29)

To clearly explain the DDHS framework for a closed loop, let us admit purely state feedback via the second HONU (18), i.e., let us define the input vector into the feedback-branch unit as follows:

$$x(k) = \begin{bmatrix} \xi_0 = 1 & \xi_2 & .. & \xi_{n_y} \end{bmatrix}^T = \begin{bmatrix} 1 \\ \hat{\mathbf{x}}(k) \end{bmatrix}$$

(30)

where $\hat{\mathbf{x}}$ is defined in (20).

Similarly, the closed loop of forward-branch recurrent HONU with feedback-branch HONU can be decomposed into state-space representation as follows:

$$\hat{\mathbf{x}}(k) = \hat{\mathbf{M}}(k-1) \cdot \hat{\mathbf{x}}(k-1) + \hat{\mathbf{N}}_{\mathbf{a}} \cdot \hat{\mathbf{d}}_{\mathbf{a}}(k-1) ;$$

$$\tilde{y}(k) = \hat{\mathbf{C}} \cdot \hat{\mathbf{x}}(k)$$

(31)

where the $\hat{\mathbf{M}}(k)$ is the LMD of the closed loop of HONUs and $\hat{\mathbf{N}}_{\mathbf{a}}(k)$ is the augmented local output matrix generally as follows:

$$\hat{\mathbf{M}}(k-1) = \hat{\mathbf{M}}\left(\hat{\mathbf{x}}, \left\{d(k-i)_{i=1...n_y}\right\}, \mathbf{w}, \mathbf{v}, k\right),$$

(32)

$$\hat{\mathbf{N}}_{\mathbf{a}}(k-1) = \hat{\mathbf{N}}_{\mathbf{a}}\left(\left\{d(k-i)_{i=1...n_y}\right\}, \mathbf{w}, \mathbf{v}, k\right)$$

(33)

where d is the external input (e.g., desired value) with further details as follows. For the particular example of a closed-loop consisting of the recurrent QNU as a forward-branch unit and the CNU as a state feedback unit, the details of the decomposed local matrix of dynamic $\hat{\mathbf{M}}$ are shown in the Appendix. The controller weights $v_{i,j,\kappa}$ and feedback gain $p(.)$ can also vary with time. Then, the augmented local output matrix yields as follows:

$$\hat{\mathbf{N}}_{\mathbf{a}} = \begin{bmatrix} & 0 \\ \mathbf{I} & \vdots \\ & 0 \\ & 1 \end{bmatrix},$$

$$\hat{\mathbf{d}}_{\mathbf{a}} = \begin{bmatrix} d(k-n_y) - p(k-n_y) \cdot v_{0,0,0}(k-n_y) \\ \vdots \\ d(k-2) - p(k-2) \cdot v_{0,0,0}(k-2) \\ d(k-1) - p(k-1) \cdot v_{0,0,0}(k-1) \\ w_{0,0} \end{bmatrix}$$

(34)

of dimension $n_y \times (n_y + 1)$ and $\mathbf{I}$ is the $n_y \times n_y$ identity matrix.

As a part of the DDHS framework, this section shows that we can apply state-space decomposition that fully preserves the nonlinearity of recurrent HONUs and their closed loops, so it can be used to define BIBS stability for these dynamical structures.

B. HONU Sliding Mode Architecture

Following the fundamentals of HONUs covered in Section II-A, this section enhances our framework to solve cases where the control objective is to achieve zero convergence, particularly with increased velocities. To develop this approach, let us consider the fundamental equations of motion for a single wheelset which is defined as follows:

$$m \cdot \ddot{y}_w = \frac{-2f_{22}}{V}\dot{y}_w + 2f_{22}\psi_w + F_y + \frac{mV^2}{R_0} + mg\vartheta - F_{c1},$$

(35)

$$I_w \cdot \ddot{\Psi}_w = \frac{-2f_{11}l\lambda}{r}y_w + \frac{-2f_{11}l^2}{V}\dot{\psi}_w + T_\Psi$$

(36)

where the longitudinal creep coefficient is lateral creep coefficient f_{22}, wheelset yaw inertia I_w, half distance of the rolling circle l, wheel conicity λ, wheelset radius r, and speed V. The control input analogically is the yaw torque of the leading wheelset $T_{\Psi 1}$; the controlled output is the leading wheelset lateral displacement $y_{w1} = y$. Then from relations (35) and (36) the states of the simplified wheelset are as follows:

$$x = \begin{bmatrix} x_1 & x_2 & x_3 & x_4 \end{bmatrix}^T = \begin{bmatrix} \dot{y}_w & y_w & \dot{\Psi}_w & \Psi_w \end{bmatrix}^T$$

(37)

where the control objective is to converge all states of both lateral and yaw displacement and velocity from (37) to zero. In similar analogy we may consider modelling the dynamics of the leading wheelset, taking into account the additional damping and stiffness characteristics from the surrounding bogie frame and trailing wheelset. Therefore, let us define the following HONU arbitrary polynomial order r as follows

$$\tilde{y}(k) = \mathbf{w}_{[0]} + \sum_{i=1}^{n} w_{[i]} \cdot x_i + \bar{\mathbf{w}} \cdot \mathrm{col}^r(\bar{\mathbf{x}})$$

(38)

where $\mathbf{w}[i]$ denotes the ith element of $\mathbf{w}$ from the very first position, e.g., $\mathbf{w}_{[0]} = w_{0,0}$ for QNU as in (14). Furthermore, $\bar{\mathbf{w}}$ represents the part of long vector $\mathbf{w}$ with corresponding (remaining) neural weights. The input vector $\bar{\mathbf{x}}$ is then chosen to model the output of lateral acceleration $\ddot{y}_{w1}$ with previous inputs of lateral and yaw displacement y_w, Ψ_w and velocity $\dot{y}_w$, $\dot{\Psi}_w$ as follows:

$$\bar{\mathbf{x}}(k) = \begin{bmatrix} x_1(k) & \cdots & x_{n_y}(k) & x_{n_y+1}(k) & \cdots & x_n(k) \end{bmatrix}^T$$

$$= \begin{bmatrix} \tilde{y}(k-n_y+1) & \cdots & \tilde{y}(k) & y_w(k-n_{y_w}+1) & \cdots & y_w(k) \end{bmatrix}$$

$$\dot{y}_w(k-n_{y_w}+1) \quad \cdots \quad \dot{y}_w(k) \quad \Psi_w(k-n_{\Psi_w}+1) \quad \cdots \quad \Psi_w(k)$$

$$\dot{\Psi}_w(k-n_{\dot{\Psi}_w}+1) \quad \cdots \quad \dot{\Psi}_w(k) \quad u(k-n_u+1) \quad \cdots \quad u(k) \end{bmatrix}^T.$$

(39)

Then, given (38), the QNU may be re-expressed via the following affine state-space representation:

$$
\bar{\mathbf{x}}(k+1) =
\begin{bmatrix}
x_1(k+1) \\
x_2(k+1) \\
\vdots \\
x_{n_y}(k+1) \\
\vdots \\
x_n(k+1)
\end{bmatrix}
$$

$$
=
\begin{bmatrix}
x_2(k) \\
x_3(k) \\
\vdots \\
x_{n_y}(k) \\
w_{[0]} + \sum_{i=1}^{n} w_{[i]} \cdot x_i + \bar{\mathbf{w}} \cdot col^r(\bar{\mathbf{x}}) \\
x_{n_y+2}(k) \\
\vdots \\
x_n(k) \\
0
\end{bmatrix}
$$

$$
+
\begin{bmatrix}
0 \\
\vdots \\
0 \\
\bar{u}(k)
\end{bmatrix}
\tag{40}
$$

where $x_i = x_i(k-1)$ and $\bar{\mathbf{x}} = \bar{\mathbf{x}}(k-1)$. We can see, conforming to affine control concept, that the state-space representation of HONUs (40) avoids the nonlinear control input terms via introduction of the new input term $\bar{u}(k)$ and generalized state variables that involves also system inputs.

Furthermore, we express the general nonlinear state-space representation of recurrent HONUs (40) into vector form with output variable as follows:

$$
\bar{\mathbf{x}}(k) = \bar{\mathbf{f}}\left(\bar{\mathbf{x}}(k-1)\right) + \bar{\mathbf{u}}(k) \; ; \; \tilde{y}(k) = x_{n_y}(k) \, . \tag{41}
$$

Then, to construct the sliding surface let us propose the following switching function:

$$
\sigma(\bar{\mathbf{x}}) = \sum_{i=1}^{n_{\bar{x}-1}} s_i \cdot \bar{x}_i(k) = s_1 \cdot \bar{x}_1(k)
$$
$$
+ s_2 \cdot \bar{x}_2(k) + \ldots + s_{n_{\bar{x}}} \cdot \bar{x}_{n_{\bar{x}}}(k) \; ;
$$
$$
\text{for} \quad s_i \in (0, 1\rangle \tag{42}
$$

where the variables s_i denote arbitrarily chosen switching weights. Then, from (42) we define the sliding mode surface where $\sigma(\bar{\mathbf{x}}) = 0$. From this, the control objective is for the trajectories in state space to converge to zero, which can be achieved if the system states are forced to push along the sliding surface, i.e., $\dot{\sigma}(\bar{\mathbf{x}}) = 0$. To find a suitable control law, let us consider the following positive-definite Lyapunov function:

$$
V(\sigma(\bar{\mathbf{x}})) = \frac{1}{2}\sigma(\bar{\mathbf{x}})^T \sigma(\bar{\mathbf{x}}). \tag{43}
$$

Then, for asymptotic stability about the origin the derivative of the Lyapunov function is defined as follows:

$$
\dot{V}(\sigma(\bar{\mathbf{x}})) = \sigma(\bar{\mathbf{x}})^T \dot{\sigma}(\bar{\mathbf{x}}) < 0 \tag{44}
$$

where

$$
\dot{\sigma}(\bar{\mathbf{x}}) = \frac{\partial \sigma(\bar{\mathbf{x}})}{\partial \bar{\mathbf{x}}} \left[\bar{\mathbf{f}}(\bar{\mathbf{x}}(k)) + \bar{\mathbf{u}}(k)\right]. \tag{45}
$$

In order to maintain the Lyapunov condition and hence the stability of the whole control law, the newly fed system inputs must be chosen so that $\dot{\sigma} < 0$ if $\sigma > 0$ and $\dot{\sigma} > 0$ if $\sigma < 0$.

Thus, on selecting the switching function defined in (42), its derivative yields

$$
\dot{\sigma}(\bar{\mathbf{x}}) = \tilde{y}(k - n_y + 2) + .. + \tilde{y}(k) + y_w(k - n_{y_w} + 1) + ..
$$
$$
+ y_w(k) + \dot{y}_w(k - n_{y_w} + 1) + .. + \dot{\Psi}_w(k - n_{\dot{\Psi}_w} + 1)
$$
$$
..\dot{\Psi}_w(k) + u(k - n_u + 2) + ..w_{0,0}
$$
$$
+ \sum_{j=1}^{n_{\bar{x}}} w_{0,j} \cdot \bar{x}_j(k) + \sum_{i=1}^{n_{\bar{x}}} \sum_{j=i}^{n_{\bar{x}}} w_{i,j} \cdot \bar{x}_i(k) + \bar{u}(k) < 0. \tag{46}
$$

On considering that the control law should follow either that $u > |\dot{\sigma}(\bar{\mathbf{x}})|$ or $u > -|\dot{\sigma}(\bar{\mathbf{x}})|$ when above the sliding surface, we may apply triangular inequality to the resultant of delayed terms for lateral displacement and angular yaw displacement as follows:

$$
[y_w(k - n_{y_w} + 1) + .. + y_w(k)] + K_1
$$
$$
\geq [y_w(k - n_{y_w} + 1) + .. + y_w(k)]
$$
$$
+ \left[\Psi_w(k - n_{\dot{\Psi}_w} + 1)..\Psi_w(k)\right]
$$
$$
\geq [y_w(k - n_{y_w} + 1) + .. + y_w(k)
$$
$$
+ \Psi_w(k - n_{\dot{\Psi}_w} + 1)..\Psi_w(k)] . \tag{47}
$$

Furthermore, the resultant of the lateral displacement velocity and angular yaw velocity respects the following:

$$
[\dot{y}_w(k - n_{y_w} + 1) + .. + \dot{y}_w(k)] + K_2
$$
$$
\geq [\dot{y}_w(k - n_{y_w} + 1) + .. + \dot{y}_w(k)]
$$
$$
+ \left[\dot{\Psi}_w(k - n_{\dot{\Psi}_w} + 1)..\dot{\Psi}_w(k)\right]
$$
$$
\geq \left[\dot{y}_w(k - n_{y_w} + 1) + .. + \dot{y}_w(k)
$$
$$
+ \dot{\Psi}_w(k - n_{\dot{\Psi}_w} + 1)..\dot{\Psi}_w(k)\right] \tag{48}
$$

where $K_1 \geq \sup(\sum \Psi_w(k))$ and $K_2 \geq \sup(\sum \dot{\Psi}_w(k))$. Then, the following control law yields, where $n_{\bar{x}_y} - 1$ is the maximum length of previously delayed output states in (37), further the term U_k denotes the sum of delayed input states in (39)

$$
\bar{u}(\bar{\mathbf{x}})=
$$
$$
\begin{cases}
\left|\sum_{i=1}^{n_{\bar{x}_y}-1} \tilde{y}(k-n_y+i)+y_w(k-n_{y_w}+i)+\dot{y}_w(k-n_{\dot{y}_w}+i)\right| \\
+K_2 + K_3 + U_k \quad if \sigma(\bar{\mathbf{x}}) < 0; \forall i \neq n_y \\
-\left(\left|\sum_{i=1}^{n_{\bar{x}_y}-1} \tilde{y}(k-n_y+i)+y_w(k-n_{y_w}+i)+\dot{y}_w(k-n_{\dot{y}_w}+i)\right|. \\
+K_2 + K_3 + U_k) \quad if \sigma(\bar{\mathbf{x}}) > 0; \forall i \neq n_y
\end{cases}
$$
$$
\tag{49}
$$

IV. STABILITY ANALYSIS

This section recalls the proof of BIBS stability for the HONU control loop based on the definition of ISS for state-space representation of nonlinear time-variant systems (Definition 1). Although a stable learning algorithm can be justified through square error criteria or further for the fundamental gradient descent algorithm in [32], its application as a constant parameter control loop or on new process dynamics must still be proven. Since the stability of the HONU sliding mode architecture has already been justified by relations (43)–(46), only the architecture in Section III-A is discussed in this section.

Definition 1 [21, Chapter 2.9]: The time-variant state-space representation of the form (52) is ISS stable provided that

$$\|\bar{\mathbf{x}}(k)\| \leq \beta(\|\bar{\mathbf{x}}(k_0)\|) + \gamma(\|u(k)\|_\infty) \quad (50)$$

where $\beta(\cdot)$ represents a κL class function which is asymptotically stable such that the function converges to a minimum for $k \to \infty$ and for a zero equilibrium that $\beta(\cdot) \to 0$; furthermore, $\gamma(\cdot)$ represents a κ_∞ class function which is unbounded and strictly increasing from a zero initial state (i.e., $\gamma = 0$ and for $k > k_0$ that $k \to \infty, \gamma \to \infty$).

Theorem 1 (DDHS): The discrete-time polynomial loops of HONUs via their decomposed state-space representation (31) are BIBS stable from initial sample time k_0 until k provided

$$S(k) = \|\hat{\mathbf{x}}(k)\| - \left\| \prod_{\kappa=k_0}^{k-1} \hat{\mathbf{M}}(\kappa) \right\| \cdot \|\hat{\mathbf{x}}(k_0)\|$$
$$- \sum_{\kappa=k_0}^{k-1} \left\| \prod_{i=\kappa}^{k-1} \hat{\mathbf{M}}(i) \cdot \hat{\mathbf{N}}_\mathbf{a}(\kappa) \right\| \cdot \|\hat{\mathbf{u}}_\mathbf{a}(\kappa)\| \leq 0 \ . \quad (51)$$

Proof: First, let us recall the proof of BIBS via Definition 1 for the general state-space representation (52) (based on papers [25] and [26]) as of a relevant class of nonlinear time-variant systems as follows; the general solution of a discrete time nonlinear state-space system is defined as follows:

$$\mathbf{x}(k) = \prod_{\kappa=k_0}^{k-1} \mathbf{A}(\kappa) \cdot \mathbf{x}(k_0) + \sum_{\kappa=k_0}^{k-1} \prod_{i=\kappa}^{k-1} \mathbf{A}(i) \cdot \mathbf{B}(\kappa) \cdot \mathbf{u}(\kappa). \quad (52)$$

Then, considering Definition 1, we take the norms of both sides and via triangular inequality it yields that

$$\|\mathbf{x}(k)\| \leq \left\| \prod_{\kappa=k_0}^{k-1} \mathbf{A}(\kappa)\mathbf{x}(k_0) \right\| + \left\| \sum_{\kappa=k_0}^{k-1} \prod_{i=\kappa}^{k-1} \mathbf{A}(i) \cdot \mathbf{B}(\kappa)\mathbf{u}(\kappa) \right\|$$
$$\leq \left\| \prod_{\kappa=k_0}^{k-1} \mathbf{A}(\kappa) \right\| \cdot \|\mathbf{x}(k_0)\| + \sum_{\kappa=k_0}^{k-1} \left\| \prod_{i=\kappa}^{k-1} \mathbf{A}(i) \cdot \mathbf{B}(\kappa)\mathbf{u}(\kappa) \right\|. \quad (53)$$

Then, considering the solution (52) as a summation of homogenous and particular solutions, and via the adoption of the BIBS discrete-time variant systems theory of [25], by setting $\hat{\mathbf{u}}_\mathbf{a}(\kappa) = 0$ where $0 \leq k_0 < k$, we may verify that

$$\|\mathbf{x}(k)\| \leq \left\| \prod_{\kappa=k_0}^{k-1} \mathbf{A}(\kappa) \right\| \cdot \|\mathbf{x}(k_0)\| \leq M_A^k \|\mathbf{x}(k_0)\| \quad (54)$$

where $M_A = \sup\{\|\mathbf{A}(k-1)\|\}$, then since due to the normalization of terms in $\mathbf{A}(k-1)$ if $M_A < 1$, as $\mathbf{x}(k) \to \mathbf{x}(k_0)$ for $k \to \infty$ about the point $\mathbf{x}(k_0)$ the system (26) is locally asymptotically stable. With respect to Definition 1, the term $\|\prod_{\kappa=k_0}^{k-1} \mathbf{A}(\kappa)\| \cdot \|\mathbf{x}(k_0)\|$ qualifies as a κL class function. Moreover, via setting $\mathbf{x}(k_0) = 0$ we may analyze the conditions of the particular solution yielding a class κ_∞ function, where the following inequality should be satisfied further for BIBS:

$$\|\mathbf{x}(k)\| \leq \left\| \sum_{\kappa=k_0}^{k-1} \prod_{i=\kappa}^{k-1} \mathbf{A}(i)\mathbf{B}(\kappa)\mathbf{u}(\kappa) \right\| \leq M_B \sum_{\kappa=k_0}^{k-1} M_A^{k-\kappa} \|\mathbf{u}(\kappa)\| \quad (55)$$

where $M_B = \sup\{\|\mathbf{B}\|\} < \infty$. If $\|\mathbf{u}(k-1)\| \leq L_u < \infty (k \geq k_0)$ then

$$\|\mathbf{x}(k)\| \leq M_B \sum_{\kappa=k_0}^{k-1} M_A^{k-\kappa} \|\mathbf{u}(\kappa)\| = \frac{M_B}{1 - M_A} \quad (56)$$

where the ratio $M_B/(1 - M_A) = L_x$ for any $\|\mathbf{u}(k-1)\| \leq L_u$, $\mathbf{x}(k) \leq L_x < \infty$ that completes the proof of Definition 1, so the time variant nonlinear discrete time system (52) is BIBS stable and; therefore, so is the representations (26) and whole HONU-MRAC control loop in (31).

Remark (Strict DDHS): Provided the discrete-time recurrent HONUs (or their loops) are BIBS stable according to Theorem 1 from the time k_0, then the BIBS stability will be strictly maintained if

$$\Delta S(k) = S(k) - S(k-1) \leq 0 \quad \text{for} \quad \forall k > k_0. \quad (57)$$

Then, in practice, we may keep k_0 be incrementally increased via settings $k_0 \leftarrow k - 2$, and it can be derived that the strict DDHS condition can be practically computed, e.g., for recurrent HONU via (57) and (58) as follows:

$$\Delta S(k) = \|\hat{\mathbf{x}}(k)\| - \|\hat{\mathbf{x}}(k-1)\| - \left\| \hat{\mathbf{B}}_\mathbf{a}(k-1) \cdot \hat{\mathbf{u}}_\mathbf{a}(k-1) \right\|$$
$$+ \left(\left\| \hat{\mathbf{A}}(k-1) \right\| - 1 \right) \cdot \left(\left\| \hat{\mathbf{A}}(k-2) \cdot \hat{\mathbf{x}}(k-2) \right\| \right)$$
$$+ \left\| \hat{\mathbf{B}}_\mathbf{a}(k-2) \cdot \hat{\mathbf{u}}_\mathbf{a}(k-2) \right\| \leq 0 \ . \quad (58)$$

V. EXPERIMENTAL SETUP

In this section, the performance as well as stability of the two proposed HONU architectures is investigated through simulation and on a real experimental railway stand (roller rig from [3], [4], [5], Fig. 5) with the considered conditions in (see Fig. 6). The experimental bogie is equipped with four contact position transducers Novotechnik TR0050 on each corner of the bogie frame, used for a direct measurement of the lateral positions of both wheelsets toward the track center and their yaw angle towards the bogie frame. An inductive sensor is further used for measuring the rotational speed of the rollers. To measure the force from the actuator yaw torque (see Fig. 1), a single axis

TABLE I
PARAMETERS OF THE WHEELSET AND BOGIE SYSTEM (ROLLER RIG)

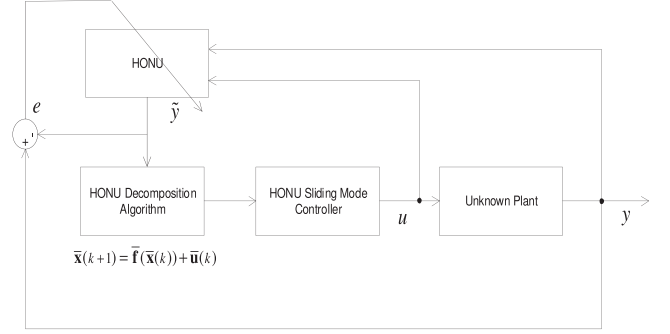| Variable	Value	Description
m	62.8 kg	Mass of an individual wheelset
m_b	150 kg	Mass of the bogie frame
f_{11}	1.35×10^5 N	Longitudinal creep coefficient (with rigid wheelset)
f_{22}	1.21×10^5 N	Lateral creep coefficient
I_w	2.9 kgm^2	Wheelset yaw inertia
I_b	9.5 kgm^2	Bogie yaw inertia
l	0.214 m	Half of rolling circle distance
l_b	0.5 m	Half wheelbase
K_w	4000 kN/m	Primary lateral stiffness
C_w	120 kN s/m	Primary lateral damping
λ	0.1	Wheel conicity
r	0.1315 m	Wheelset radius
w	0.550 m	Span of steering linkages
c_{f1}	0.3	Frictional coefficient factor

Fig. 4   HONU sliding mode architecture where one HONU is used as a static online adaptive model for plant identification.
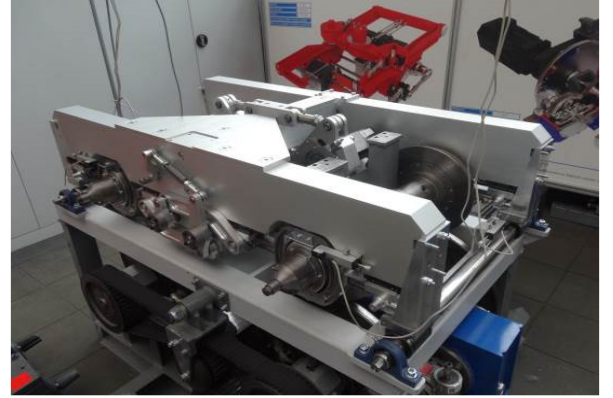

Fig. 5   Czech Technical University (CTU) Roller-Rig for running straight and curved track sections with IRW and conventional wheelset configurations.
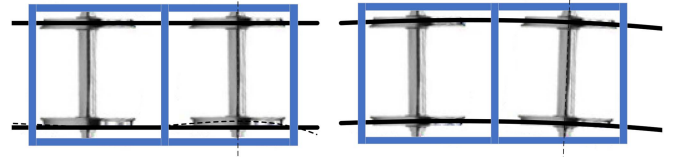

Fig. 6.   (Left)—Tested conditions due to misalignment on track (or track irregularities, notice the dashed black line), (right)—Constant track curve.

compression load cell Omegadyne LC304-1K with load capacity 4448 N and accuracy $\pm 0.5\%$ FSO is used.

The output signals of sensors and the driving voltage signals for the actuators are sent via an I/O card Humusoft MF634 installed in a standard PC. All signal processing is executed in a real time using MATLAB Simulink with real-time control and signal processing toolbox. The signals from all sensors are filtered, differentiated, and further processed to calculate the corresponding inputs for actuator control. Table I depicts the main parameters of the experimental bogie stand.

A. Control of Zero Lateral Displacement for Conventional Wheelset via HONU Sliding Mode Architecture

Following derivation of the proposed HONU sliding mode architecture in Section III-B, this section experimentally analyzes the performance of the approach at various roller velocities for the setup in Section V. At first, as per Fig. 4, a static QNU (i.e., $r = 2$) trained via RLS learning is applied with a learning rate set to 0.395. The delayed samples of lateral displacement and its derivative (velocity) are set to $n_{y_w}, n_{\dot{y}_w} = 2$, respectively. Then, the previous samples of angular displacement and its derivative (velocity) are set to $n_{\Psi_w}, n_{\dot{\Psi}_w} = 2$ and previous inputs (yaw torque) is $n_u = 2$.

The proposed approach is first analyzed in order to compare with the benchmark result for a conventional wheelset setup on a straight track section with leading wheelset control from paper [8], see Fig. 2. In Fig. 7 here it is clearly illustrated that after 6 s for the same parameters, all states converge to zero and the hunting motion is almost fully eliminated with ± 44.9 N·m limiting servo motor torque and 0.1 s period between switching inputs, 4 s faster than in [8]. From this result, the successful

convergence of all wheelset states is seen within $t = 6$ s where almost superimposed identification from the HONU is shown in comparison with the real lateral acceleration for which it models. This also shows the versatility of the algorithm with rapid online identification via RLS to identify the contemporary dynamics of the wheelset system without need of adjustment for the controller parameters.

To justify robustness of the approach for real applications, a track curving scenario is simulated in Fig. 8. Here, a continuous track section with respective track curvature radii from Fig. 6 (right) of $R_0 = 1000, 250$, and 400 m is illustrated. Furthermore, the section with $R_0 = 250$ m introduces a 0.1 radian track cant between 10 and 20 s. As can be seen, the control algorithm is able to negotiate constant track curving with almost no observable
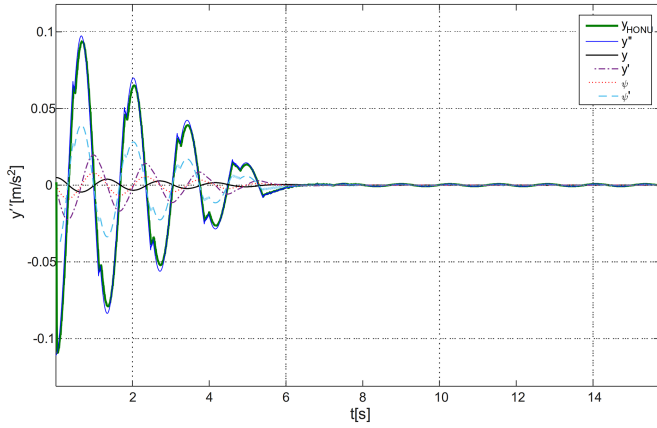
Fig. 7. Convergence of states within 6 s (for 50 r/min) with HONU sliding mode controller on roller rig simulation, via RLS training on a static QNU.
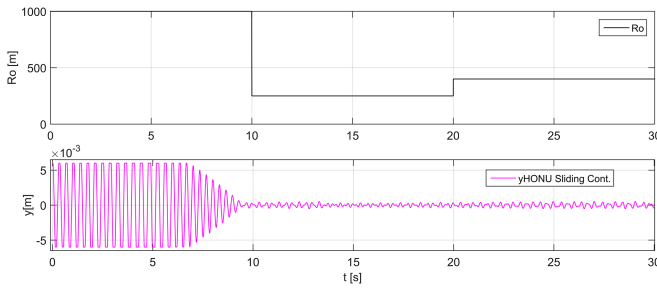

Fig. 8. Negotiation track curving from 5 s at 100 rpm ($R_0 = 1000$ m, 250 m with 0.1 radians track cant, 400 m) with HONU sliding mode controller on roller rig simulation.

deviation in the minimized lateral displacement between the track curve transitions or due to introduced track cant.

Next, Fig. 9 investigates the performance of the proposed control algorithm with respect to gradually increasing rotational velocities. To simulate motion of the bogie frame along rail tracks the asynchronous roller drives are incrementally increased to 60, 100, and 150 r/min, respectively.

In Fig. 9(a), a comparison with a derived HONU-MRAC as a dynamic QNU model with QNU feedback controller where $n_{qy} = 4, n_{qu} = 5$ and adaptive RLS learning is shown for 60 r/min. Although the roller rig exhibits pronounced hunting motion between ± 4.5 mm of lateral displacement within the first 6 s, the HONU sliding mode controller can stabilize the hunting motion 10 s faster than the applied HONU-MRAC configuration. When monitoring the neural weights using RLS training, it is clear the learning is stable with the convergence of all weights within 250 samples, with 0.002 s of applied sensor sampling, where the HONU-MRAC requires one order slower sampling for the same hardware. Given this result, the rotational speed is increased to 100 and 150 r/min, respectively. From Fig. 9(b) and (c) although the initial stages of application show higher jittering in the hunting motion characteristic as compared with lower revolutions of the rollers remarkably within 5 s it is almost fully dissipated and stabilizes the roller

rig lateral displacement to fully converge to zero where in comparison to the HONU-MRAC configuration, the effects of hunting motion are still pronounced throughout application of the control algorithm. Furthermore, the convergence of all neural weights for the HONU sliding mode controller is achieved within the same frame of samples as compared to the result at 60 r/min, even with the faster dynamic response at higher speeds.

B. Active Control for Setpoint of Lateral Displacement With Conventional Wheelset Configuration via HONU-MRAC

To further analyze the control performance and stability of HONUs, a different control objective is investigated, which is to track a desired setpoint of lateral displacement due to effects such as bogie yaw or track irregularities as in Fig. 6(left). To solve this control objective, the two-HONU closed-loop architecture (as in Fig. 3) is chosen. We implement the classical MRAC scheme for HONUs, where the forward-branch HONU can incrementally adapt its weights $\mathbf{w}(k) = \mathbf{w}(k - 1) + \Delta\mathbf{w}(k)$ to approximate the real plant. The feedback-branch HONU can then incrementally adapt its weights $\mathbf{v}(k) = \mathbf{v}(k - 1) + \Delta\mathbf{v}(k)$ to minimize some control error criteria based on the following reference error:

$$e_{\text{ref}}(k) = y_{\text{ref}}(k) - y(k) \cong y_{\text{ref}}(k) - \tilde{y}(k) \tag{59}$$

where $y_{\text{ref}}(k)$ is the output of a reference model that has the desired user-defined dynamics, and the feedback-branch HONU is the controller for desired dynamics. In the next example, a further experimental analysis for comparison of the DDHS stability conditions to the Lyapunov-function technique is presented to justify stability of the control law of a two-HONU control loop itself. In particular, if the feedforward-branch HONU (plant) is not adapted, i.e., $\mathbf{w}(k) = \text{const}$ and if the feedback-branch HONU (controller) is incrementally adapted as $\mathbf{v}(k) = \mathbf{v}(k - 1) + \Delta\mathbf{v}(k)$, then the desired equilibrium means both zero reference error (59) and converged controller weights $\Delta\mathbf{v}(k) = 0$. Then, for the control loop, the Lyapunov function with the stability condition yields for validating the stabilization of the applied control law

$$V(k) = e_{\text{ref}}(k)^2 + \Delta\mathbf{v}(k)\Delta\mathbf{v}(k)^T; \Delta V(k)$$
$$= V(k) - V(k - 1) < 0. \tag{60}$$

However, as seen in Fig. 10 the strict DDHS condition is superior in earlier detection of unstable dynamics, making it advantageous for higher speed control.

Although used for analysis of the HONU-MRAC architecture, in similar analogy this is also applicable to justify stability and robustness of the adaptive HONU as part of the HONU Sliding mode architecture. Though as long as the learning algorithm is stable, the global asymptotic stability via sliding mode is ensured by (43)–(46). To further justify the robustness of HONUs in adaptation of changed process dynamics, Fig. 11 shows real-time stable adaptation of the whole control loop through all setpoints.
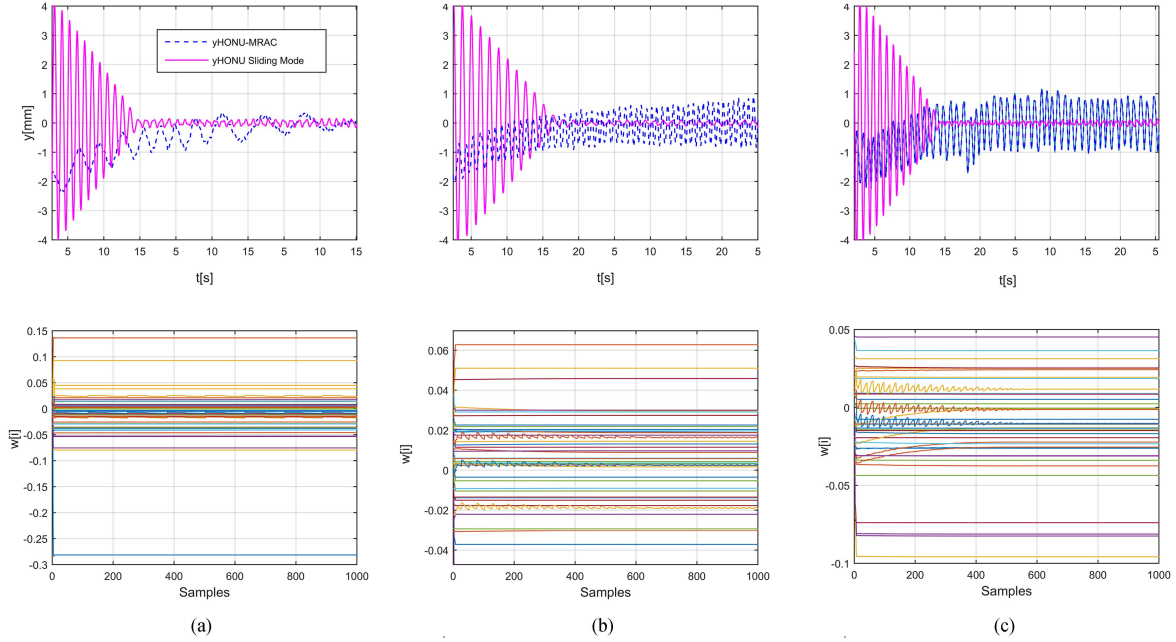
Fig. 9. Comparison of HONU sliding mode control and cascade PI with HONU-MRAC (QNU-QNU) with pre-training via RLS on real roller rig with straight track for higher velocities (a) 60 r/min of rotational speed and convergence of sliding mode controller weights via RLS, (b) 100 r/min, (c) 150 r/min.
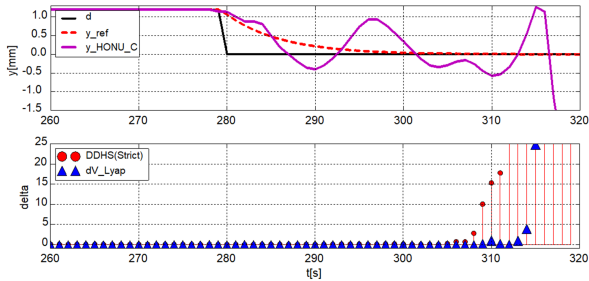

Fig. 10. (Top): stability analysis: response with unstable incremental learning of QNU controller on roller rig simulation at $t > 280s$. (Bottom): the Lyapunov validation of control-law stability $\Delta V \leq 0$ (60) compared with strict DDHS stability condition $\Delta S \leq 0$ (57) which more clearly shows unstable dynamics.
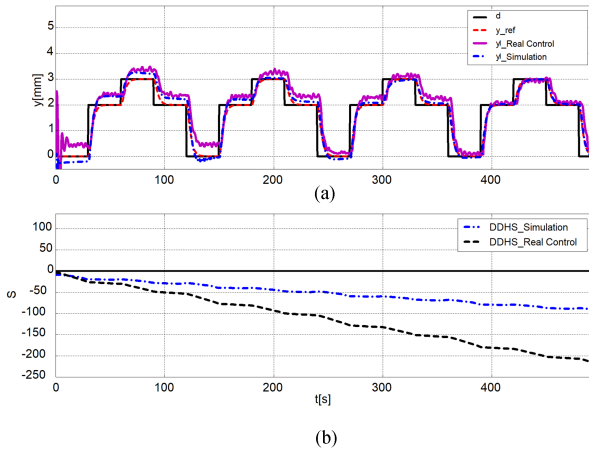

Fig. 11. DDHS. (a) HONU-MRAC performance with real and also simulated bogie on straight track (due to changed stiffness and damping characteristics in bogie frame). (b) DDHS stability condition (for $k_0 = 0$).
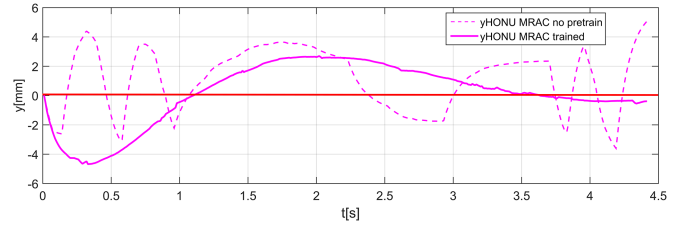

Fig. 12. Comparison of standalone adaptive HONU-MRAC control architecture on real roller rig at 50 r/min with pretraining from dataset in Fig. 11 and no pretraining on straight track.

VI. DISCUSSION

Naturally as shown in Section V, the basis of good control performance is in the identification of the process dynamics in real time. This requires the process to be stable for a minimal sufficient set of training data to identify and initiate control of the wheelset. In applications where the systems dynamics is truly unknown, i.e., neither model nor training data exists in advance, a data-driven control loop with model identification must adapt quickly to process dynamics. This may be not ideal for layered or the two-HONU control architectures with common hardware. Further research can be in the use of faster hardware, e.g., FPGA or switch-OFF of the algorithm once trained to minimize computational overload. An example of this can be batch or minibatch learning algorithms. Fig. 12 compares this problem at 50 r/min with a standalone fully adaptive two-HONU (QNU-QNU) control loop. Here, without sufficient pretraining, the control loop must rapidly identify the system dynamics in real time to account for bogie yaw (see Fig. 6 left). Although with pretraining and fast nonlinear architecture, the response shows desirable convergence toward zero at 50 r/min (see Fig. 12),

$$\hat{\mathbf{M}}(k-1) = \hat{\mathbf{A}}(k-1) - \hat{\mathbf{B}}(k-1) \cdot \begin{bmatrix} p(k-n_y) \cdot \left[v_{0,0,1} + \sum_{j=1}^{n_y} \sum_{\kappa=j}^{n_y} v_{1,j,\kappa} \cdot x_j \cdot x_\kappa \right. \\ \vdots \\ p(k-2) \cdot \left[v_{0,0,1} + \sum_{j=1}^{n_y} \sum_{\kappa=j}^{n_y} v_{1,j,\kappa} \cdot x_j \cdot x_\kappa \right. \\ p(k-1) \cdot \left[v_{0,0,1} + \sum_{j=1}^{n_y} \sum_{\kappa=j}^{n_y} v_{1,j,\kappa} \cdot x_j \cdot x_\kappa \right. \end{bmatrix}$$

$$\left. v_{0,0,2} + \sum_{j=2}^{n_y} \sum_{\kappa=j}^{n_y} v_{2,j,\kappa} \cdot x_j \cdot x_\kappa \; \cdots \; v_{0,0,n_y} + v_{n_y,n_y,n_y} \cdot x_{n_y}^2 \right]$$
$$\vdots$$
$$\left. v_{0,0,2} + \sum_{j=2}^{n_y} \sum_{\kappa=j}^{n_y} v_{2,j,\kappa} \cdot x_j \cdot x_\kappa \; \cdots \; v_{0,0,n_y} + v_{n_y,n_y,n_y} \cdot x_{n_y}^2 \right]$$
$$\left. v_{0,0,2} + \sum_{j=2}^{n_y} \sum_{\kappa=j}^{n_y} v_{2,j,\kappa} \cdot x_j \cdot x_\kappa \; \cdots \; v_{0,0,n_y} + v_{n_y,n_y,n_y} \cdot x_{n_y}^2 \right] \cdot \qquad (61)$$

though functional, there is much greater hunting motion at higher speeds than with the sliding mode in Fig. 9.

Thus, the proposed HONU-sliding mode architecture is superior with this type of control challenge as it only requires training of one HONU which is computationally much faster instead of two for process identification and then a feedback controller which reflects the reason why at higher speeds, the HONU-MRAC architecture is not reacting quickly enough to converge to the tracking point, even with adequate pretraining.

VII. CONCLUSION

From this work, two HONU based architectures were investigated for railway wheelset active control. Using ISS an efficient stability analysis method DDHS/DDHS(Strict) was derived to ensure fast detection for violation of BIBS stability, which was superior to the Lyapunov algorithm in Fig. 10 and can also be extended to other time-variant in-parameter-linear nonlinear learning systems. For higher rotational speeds, the HONU sliding mode controller shows its potential in outperforming the benchmark HONU-MRAC (see Fig. 9), with its potential for rapid correction of the wheelset lateral displacement and reduced hunting motion. This is due to fast computation of a single HONU problem and hard control reaction in the opposite direction of yaw whilst maintaining adhesion to the sliding surface for zero convergence of the resulting wheelset states. From the relations (43)–(46), global asymptotic and further BIBS stability is also ensured for all control inputs applied to the control loop. Based on a data-driven method, intermediate system dynamics can be identified even with limited measurement of all dynamical states or precise mathematical descriptions, making such an approach advantageous to conventional control approaches.

APPENDIX

A. Local Matrix of Dynamics (LMD) for Polynomial Decomposition for Closed Loop of HONUs—DDHS

The $n_y \times n_y$ LMD of a QNU-CNU can be expressed as follows: (61) shown at the top of this page.

REFERENCES

[1] R. M. Goodall and W. Kortum, "Mechatronic developments for railway vehicles," *Elsevier*, vol. 10, no. 8, pp. 887–898, Aug. 2002, doi: 10.1016/S0967-0661(02)00008-4.

[2] S. Bruni, R. M. Goodall, T. X. Mei, and H. Tsunashima, "Control and monitoring for railway vehicle dynamics," *Int. J. Veh. Mechanics Mobility*, vol. 45, nos. 7/8, pp. 743–779, 2007.

[3] J. Kalivoda and P. Bauer, "Design of experimental mechatronic bogie," in *Proc. Int. Symp. Seed-Up Service Technol. Railway Maglev Syst.*, 2015, doi: 10.1299/jsmestech.2015.1F34-1_.

[4] J. Kalivoda and P. Bauer, "Mechatronic bogie for roller rig tests," in *Proc. 24th Int. Symp. Dyn. Veh. Roads Tracks*, 2015.

[5] S. Myamlin, J. Kalivoda, and L. Neduzha, "Testing of railway vehicles using roller rigs," *Procedia Eng.*, vol. 187, pp. 688–695, 2017, doi: 10.1016/j.proeng.2017.04.439.

[6] J. Kalivoda, P. Bauer, and Z. Novak, "Assessment of active wheelset steering system using computer simulations and roller rig tests," *Appl. Sci.*, vol. 11, Dec. 2021, Art. no. 11727, doi: 10.3390/app112411727.

[7] R. M. Goodall and C. P. Ward, "Active control of railway bogies - assessment of control strategies," in *Proc. Int. Symp. Speed-Up Sustain. Technol. Railway Maglev Syst.*, 2015.

[8] J. Kalivoda and P. Bauer, "Roller rig tests with active stabilization of a two-axle bogie," in *Proc. Civil Comp Railways*, 2016.

[9] F. Braghin, S. Bruni, and F. Resta, "Active yaw damper for the improvement of railway vehicle stability and curving performances: Simulations and experimental results," *Int. J. Veh. Mechanics Mobility*, vol. 44, no. 11, pp. 857–869, 2006, doi: 10.1080/00423110600733972.

[10] P. Urda, J. F. Aceituno, S. Munoz, and J. L. Escalona, "Artificial neural networks applied to the measurement of lateral wheel-rail contact force: A comparison with a harmonic cancellation method," *Mech. Mach. Theory*, vol. 153, 2020, Art. no. 103968, doi: 10.1016/j.mechmachtheory.2020.103968.

[11] R. Cespi, R. Galluzzi, R. A. Ramirez-Mendoza, and S. Di Gennaro, "Artificial intelligence for stability control of actuated in–wheel electric vehicles with carsim validation," *Mathematics*, vol. 9, 2021, Art. no. 3120, doi: 10.3390/math9233120.

[12] B. Chen, K. Liu, X. Liu, P. Shi, C. Lin, and H. Zhang, "Approximation-based adaptive neural control design for a class of nonlinear systems," *IEEE Trans. Cybern.*, vol. 44, no. 5, pp. 610–619, May 2014.

[13] H. Wang, K. Liu, X. Liu, B. Chen, and C. Lin, "Neural-based adaptive output-feedback control for a class of nonstrict-feedback stochastic nonlinear systems," *IEEE Trans. Cybern.*, vol. 45, no. 9, pp. 1977–1987, Sep. 2015.

[14] W. Meng, Q. Yang, J. Si, and Y. Sun, "Adaptive neural control of a class of output-constrained nonaffine systems," *IEEE Trans. Cybern.*, vol. 46, no. 1, pp. 85–95, Jan. 2016.

[15] I. Bukovsky, N. Homma, L. Smetana, R. Rodriguez, M. Mironovova, and S. Vrana, "Quadratic neural unit is a good compromise between linear models and neural networks for industrial applications," in *Proc. IEEE 9th Int. Conf. Cogn. Informat.*, 2010, pp. 556–560, doi: 10.1109/COGINF.2010.5599677.

[16] B. Xu and F. Sun, "Composite intelligent learning control of strict-feedback systems with disturbance," *IEEE Trans. Cybern.*, vol. 48, no. 2, pp. 730–741, Feb. 2018.

[17] B. Xu, Z. Shi, C. Yang, and F. Sun, "Composite neural dynamic surface control of a class of uncertain nonlinear systems in strict-feedback form," *IEEE Trans. Cybern.*, vol. 44, no. 12, pp. 2626–2634, Dec. 2014.

[18] R. J. Williams and D. Zipser, "A learning algorithm for continually running fully recurrent neural networks," *Neural Comput.*, vol. 1, no. 2, pp. 270–280, Jun. 1989, doi: 10.1162/neco.1989.1.2.270.

[19] P. J. Werbos, "Backpropagation through time: What it does and how to do it," *Proc. IEEE*, vol. 78, no. 10, pp. 1550–1560, Oct. 1990.

[20] P. M. Benes, I. Bukovsky, M. Cejnek, and J. Kalivoda, "Neural network approach to railway stand lateral SKEW control," in *Comput. Sci. Inform. Technol.*, Sydney, Australia: Academy & Industry Research Collaboration Center (AIRCC), Feb. 2014, pp. 327–339, doi: 10.5121/csit.2014.4228.

[21] P. Benes, I. Bukovsky, and J. Kalivoda, "Achievements in neural network approach to railway stand lateral skew control," *Nové metody a postupy v oblasti přístrojové a řídicí techniky - U12110*, Herbertov, Czech Republic: Czech Technical University in Prague, May 2014.

[22] J. Fei and C. Lu, "Adaptive sliding mode control of dynamic systems using double loop recurrent neural network structure," *IEEE Trans. Neural Netw. Learn. Syst.*, vol. 29, no. 4, pp. 1275–1286, Apr. 2018.

[23] P. Benes and I. Bukovsky, "On the intrinsic relation between linear dynamical systems and higher order neural units," in *Intelligent Systems in Cybernetics and Automation Theory*, R. Silhavy, R. Senkerik, Z. K. Oplatkova, Z. Prokopova, and P. Silhavy, Eds. Berlin, Germany: Springer, 2016. [Online]. Available:http://link.springer.com/chapter/10.1007/978-3-319-18503-3_27

[24] I. Bukovsky, P. M. Benes, and M. Vesely, "Introduction and application aspects of machine learning for model reference adaptive control with polynomial neurons," in *Proc. Artif. Intell. Mach. Learn. Appl. Civil, Mech., Ind. Eng.*. Hershey, PA, USA: IGI Global, 2020, pp. 59–84.

[25] A. Bacciotti and A. Biglio, "Some remarks about stability of nonlinear discrete-time control systems," *Nonlinear Differ. Equ. Appl.*, vol. 8, no. 4, pp. 425–438, Apr. 2000, doi: 10.1007/PL00001456.

[26] E. D. Sontag, "Input to state stability: Basic concepts and results," in *Nonlinear and Optimal Control Theory*, vol. 1932. Berlin, Germany: Springer, 2008, pp. 163–220.

[27] H. Selamat and M. A. Zawawi, "Optimal controller design for a bogie-based railway vehicle," in *Stud. Autom. Control Ground Vehicles*, 1st ed. Penerbit Universiti Teknologi Malaysia, Malayisia: Univision Press Sdn. Bhd, 2007, pp. 15–30.

[28] B. Liang and S. D. Iwnicki, "Independently rotating wheels with induction motors for high-speed trains," *J. Control Sci. Eng.*, vol. 2011, 2011, Art. no. 7, doi: 10.1155/2011/968286.

[29] O. Polach, "Characteristic parameters of nonlinear wheel/rail contact geometry," *Int. J. Veh. Mechanics Mobility*, vol. 48, pp. 19–36, Aug. 2009, doi: 10.1080/00423111003668203.

[30] J. Musilek, "Horizontal forces on crane runway caused by skewing of the crane," *IOP Conf. Ser., Mater. Sci. Eng.*, vol. 471, no. 5, Jun. 2018, Art. no. 052001, doi: 10.1088/1757-899X/471/5/052001.

[31] "Eurocode 1 - Actions on Structures - Part 3: Actions Induced by Cranes and Machinery," EN 1991-3, Jul. 2006.

[32] I. Bukovsky and N. Homma, "An approach to stable gradient-descent adaptation of higher order neural units," *IEEE Trans. Neural Netw. Learn. Syst.*, vol. 28, no. 9, pp. 2022–2034, Sep. 2017.

Peter Mark Benes received the Ph.D. degree in control and systems engineering from Czech Technical University in Prague, Prague, Czech Republic, in 2020.

He is currently with the Rail Automation Division R&D, Siemens Mobility s.r.o., Prague. His research interest includes adaptive systems for railway and automation systems and in-parameter-linear nonlinear polynomial neural architectures for process control.

Ivo Bukovsky (Senior Member, IEEE) received the Ph.D. degree in control and systems engineering from the Czech Technical University (CTU) in Prague, Czech Republic, the in 2007.

He was a short-term visiting Researcher with the University of Saskatchewan (2003) and the University of Manitoba (2010) in Canada. Since 2009, he has been cooperating with Tohoku University, Sendai, Japan. He is fully with the Department of Computer Science at the Faculty of Science of the University of South Bohemia in České Budějovice and partly with the Dpt. of Mechanics, Biomechanics and Mechatronics at the Faculty of Mechanical Engineering of the CTU in Prague. His research interests include novelty detection, multiscale analysis approaches, dynamical systems and data analysis, adaptive control with in-parameter-linear nonlinear neural architectures, and novel information theory through machine learning.

Dr. Bukovsky served as an Associate Editor for IEEE TRANSACTIONS ON NEURAL NETWORKS, IEEE TRANSACTIONS ON NEURAL NETWORKS AND LEARNING SYSTEMS, and IEEE TRANSACTIONS ON CYBERNETICS as well as PC for numerous IEEE conferences.